# A J INTEGRAL BASED METHOD TO MEASURE FRACTURE RESISTANCE AND COHESIVE LAWS IN MATERIALS EXHIBITING LARGE SCALE PLASTICITY

B. F. Sørensen* and S. Goutianos

*Department of Wind Energy, Section of Composites and Materials Mechanics, Technical University of Denmark, Risø Campus, DK-4000 Roskilde, Denmark*
**bsqr@dtu.dk*

**Keywords:** *J* Integral; Cohesive Law; Non-Linear Material, Plasticity

## Abstract

*A method is developed to extract the fracture resistance and mode I cohesive law of non-linear elastic-plastic materials using a Double Cantilever Beam (DCB) sandwich specimen loaded with pure bending moments. The method is based on the J integral which is valid for materials having a non-linear stress-strain relationship as long as there is no unloading at any material point. A numerical parameter study is performed for a wide range of material and specimen parameters to examine the accuracy of the method. In the range examined, the error of the method is less than 11% and thus it can be used to measure the fracture resistance experimentally and determine the mode I cohesive law including its shape.*

## 1. Introduction

Linear elastic fracture mechanics (LEFM) is applicable when the fracture process zone is very small in comparison with all length dimensions (including the crack size) of a component [1]. In this case, the fracture process zone is embedded within a universal crack tip stress field (the so-called K-dominant zone). In contrast, when the size of the fracture process zone is comparable to or larger than any relevant specimen dimension, the fracture process zone should be modeled by non-linear fracture mechanics e.g. by a cohesive zone model [2,3]; describing the fracture process of materials through a traction separation relationship as shown in Fig. 1.

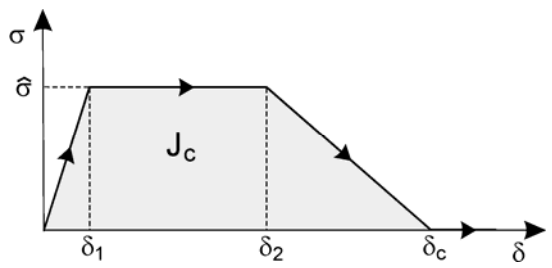


**Figure 1.** Schematic illustration of the idealized cohesive law used in this study. $J_c$ is the mode I work of separation, $\delta_c$, the critical separation, the opening at complete failure, and $\hat{\sigma}$ is the peak traction.

Since Needleman [4] introduced a mode I cohesive law in a continuum mechanics finite element model, cohesive zone modeling have been widely used in advanced numerical

models of materials and structures e.g. [5,6]. Despite the widespread use of the cohesive laws in simulations, there are relative few studies on experimental determination of cohesive laws. Usually, the cohesive laws are determined indirectly by comparing experimentally measured specimen response (e.g. overall load-displacement relationships) with model predictions for a number of cohesive law parameters through an iterative guessing process [7]. This approach usually requires extensive computational effort to extract the cohesive law parameters and the shape of the cohesive laws is pre-defined and not an outcome from the experiments.

A small number of experimental methods have been developed to determine cohesive laws directly [8,9]. For example Brenet at al. [9] used the so-called direct tension test where by measuring the displacement between two points across the failure plane, the opening of the cohesive law in principle can be measured. However, in practice, the separation is not always uniform across the width of the specimen. Thus, it can be argued that these techniques are either involved and/or it is difficult to achieve the correct conditions. A different approach is to obtain the cohesive law from measurements of the path independent $J$ integral [10] and the end-opening of the cohesive zone as proposed by Li and Ward [11]:

$$\sigma = \frac{dJ}{d\delta^*} \tag{1}$$

where $J$ is the value of the $J$ integral and $\delta^*$ is the end-opening, i.e., the normal opening at the end of the fracture process zone. The J-integral must be analyzed along the external boundaries of the specimen to establish connection with the overall geometry and loading. The $J$ integral approach is valid also for problems involving large-scale bridging and a closed form analytical J-integral solution has been derived for the double cantilever beam (DCB) specimen loaded with pure bending moments [12]. Using this specimen Sørensen and Jacobsen [13] measured the mode I bridging/cohesive laws directly using Eq. 1.

The studies mentioned above assume that the material outside the fracture process zone is elastic. However, many materials e.g. metals, polymers, composites have a non-linear material response that needs to be taken into account [5,6]. Thus, the idea of the present work is to explore if it is possible to extent the approach of Sørensen and Jacobsen [13] for materials that exhibit large scale yielding. We think that the DCB loaded with pure bending moments could be a suitable test specimen since a monotonic increase in the J-integral also requires a monotonic increase in the applied bending moments. This specimen will not experience global unloading during crack growth. We hope that this specimen may only undergo a small amount of unloading around the fracture process zone during crack propagation so that the $J$ integral approach can be used and consequently the fracture resistance and the cohesive law can be determined relatively accurate from experimental measurements.

## 2. $J$ integral approach for non-linear material

Fig. 2 shows the double cantilever beam (DCB) sandwich specimen loaded with pure bending moments used. The non-linear material is fixed to elastic beams. The thickness of the non-linear material is $2h$, and the thickness of each elastic beam is $H$. The fracture process is described by a trapezoidal cohesive law (see Fig. 1). Material #1 is taken to be linear elastic:

$$\sigma_{11}^{\#1} = E^{\#1}\varepsilon_{11} \tag{2}$$

where $E^{\#1}$ is the Young's modulus of material #1. Material #2 has a non-linear stress-strain law representing plasticity i.e. plasticity may form at the crack tip and in the beams (large scale yielding):

$$\sigma_{11}^{\#2} = E^{\#2}\varepsilon_{11} + a_2\varepsilon_{11}^2 \tag{3}$$

With this specific formulation, the $J$ integral can be calculated analytically. However, the method developed here is fairly general since numerical methods can be used for other non-linear stress-strain relations when it is not possible to derive a closed-form solution for the $J$ integral.

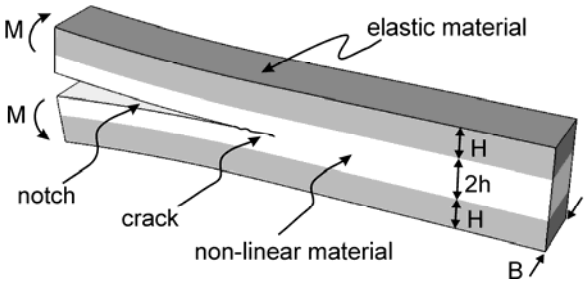


**Figure 2.** Double Cantilever Beam (DCB) sandwich specimen loaded with pure bending moments.

Due to symmetry only the upper half of the specimen (see Fig. 2) is considered next. Since the beam-ends are subjected to pure bending moments, the normal strain $\varepsilon_{22}$ varies linearly across the height of the specimen as shown in Fig. 3:

$$\varepsilon_{11} = \frac{\hat{\varepsilon}}{\Delta} y \quad \text{for} \quad \Delta - H - h \le y < \Delta \tag{4}$$

where $\hat{\varepsilon}$ is the strain at the top of the upper beam (#1), $\varepsilon_{22}(y = \Delta) = \hat{\varepsilon}$. The other parameters, $H$, $h$, $\Delta$ and the $y$ coordinate axis are defined in Fig. 3.

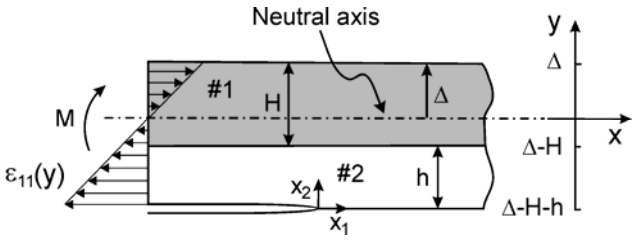


**Figure 3.** Strain variation across the thickness of the upper half of the DCB specimen. $\Delta$ is the neutral axis in the local $x - y$ coordinate system.

It can be shown that the moment equilibrium for the upper half specimen, using Eqs. 2-4, leads to [14]:

$$A\hat{\varepsilon}^2 + B\hat{\varepsilon} + C = 0 \tag{5}$$

where the non-dimensional parameters $A$ and $B$ depend only on material properties and geometry [14], whereas $C$ is given by:

$$C = -\frac{M}{BH^2 E^{\#1}} \tag{6}$$

Thus, $\hat{\varepsilon}$ can be computed analytically as a function of the applied moment, $M$. In the above it assumed that the position of the neutral axis does not translate with increasing the loading.

The $J$ integral is calculated then along a path ($\Gamma_i$ with $i = 1,5$) along the external boundaries of the specimen as shown in Fig. 4. It can be shown, following the procedure in [14], that $J$ integral equals:

$$J_{ext} = 2J_5 \tag{7}$$

where $J_5$ is the $J$ integral along the external boundaries of the upper half of the DCB specimen and is given by:

$$J_5 = \frac{\mathrm{E}^{\#1}\hat{\varepsilon}^2}{2\Delta^2}(\Delta^2 H - \Delta H^2 + \frac{H^3}{3}) + \frac{\mathrm{E}^{\#2}\hat{\varepsilon}^2}{2\Delta^2}(\frac{h^3}{3} + h^2(\Delta - H - h) + h(\Delta - H - h^2) + \frac{2a_2\hat{\varepsilon}^3}{3\Delta^3}(\frac{h^4}{4} + h^3(\Delta - H - h) + \frac{3h^2}{2}(\Delta - H - h)^2 + h(\Delta - H - h)^3) \tag{8}$$

In summary, by the use of (7) and (8), $J_{ext}$ can be calculated from $\hat{\varepsilon}$ which again is a function of the applied moment, $M$ through (5) and (6).

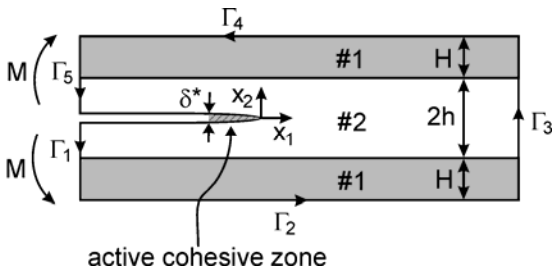


**Figure 4.** Two-dimensional specimen representation and $J$ integral path along the external boundaries.

The $J$ integral is calculated along a local integration path that encloses the fracture process zone [10,12]:

$$J_{loc} = \int_0^{\delta^*} \sigma(\delta) d\delta \tag{9}$$

Differentiation of Eq. 7 gives Eq. 1. Since $J$ integral is path independent as long as there is no unloading in any material point, $J_{ext}$ from Eq. (7) equals $J_{loc}$ of Eq. (9). Thus the cohesive law, including the shape, can be directly obtained from experiments by measuring the applied moment and the end-opening at the end of the fracture process zone.

## 3. Numerical model

The finite element method was used to examine the accuracy of the $J$ integral approach developed in the previous Section using the commercial finite element code Abaqus. The DCB specimen was modeled as a 2D plane stress problem. Crack initiation and growth was modeled using cohesive elements available in Abaqus. In the finite element calculations, the crack tip position was defined as the position within the fracture process zone where the opening equals $\delta_1$, or the traction is equal to the peak traction value $\hat{\sigma}$, (see Fig. 1 for definition of symbols).

$$\sigma_i = \frac{J_{R_i} - J_{R_{i-1}}}{\delta_i^* - \delta_{i-1}^*} \tag{10}$$

From the finite element calculations, the end-opening, $\delta^*$, was extracted as a function of the applied moment, $M$. Then, the $J$ integral (Eq. (7)) was computed. With $J_R$ (fracture resistance) and $\delta^*$ available, the cohesive law was calculated from Eq. 1. The differentiation of $J - \delta^*$ was done directly on the numerical data and not on fitted data as shown in Eq. (10) where $i$ represents increments of applied moment. The differentiation of Eq. (10) introduces noise to the predicted cohesive law since Abaqus explicit used. Mass scaling was applied in order to obtain a quasi-static solution.

For each case solved, the numerically obtained fracture resistance and cohesive law are then compared with the fracture energy and cohesive law originally specified in the finite element model. If the proposed approach is accurate, then the difference between the two fracture energies and cohesive laws should be small.

## 4. J-integral approach verification

Fig. 5 shows the fracture resistance, calculated from $M$ (extracted from the finite element model), using Eq. 5 for three different cohesive laws ($\delta_2$ varies while all other openings and the peak tractions are the same). The dotted lines represent the fracture resistance curves obtained by integrating the cohesive laws (Fig. 1) specified in the finite element model. It can be seen that the steady-state fracture resistance, $J_{ss}$, for each cohesive law is slightly higher than the corresponding work of separation and that the steady-state is attained at an end-opening larger than $\delta_c$. A higher $J_{ss}$ is expected as there is a small region where the material unloads behind the crack tip. The difference in the fracture resistance is less than 10% for the three cohesive laws.

Fig. 6 shows the corresponding predicted cohesive laws (solid lines) whereas the dashed lines represent the cohesive laws specified in the finite element model. Despite the noise in the numerical results (see previous Section), the computed cohesive laws agree well with the input cohesive laws. The peak traction value and cohesive law shapes are well captured. The differences between the computed and expected cohesive law parameters are less than 11%.

In the rest of the Section some selected results are given to show the effect of few non-dimensional parameters describing the problem of Fig. 2 on the predicted fracture resistance.

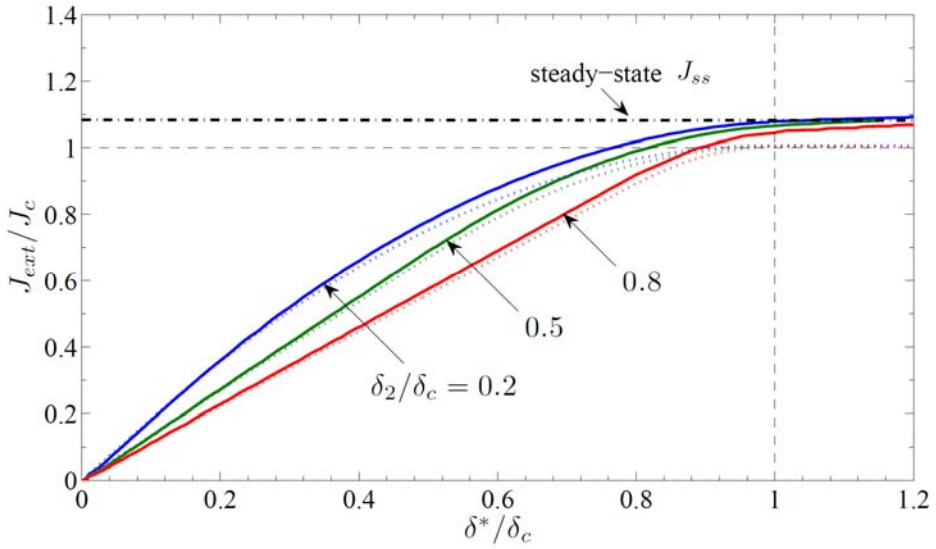


**Figure 5.** $J_R$ versus $\delta^*$ for various $\delta_2$ where $J_R$ is calculated from $M$ using Eq. 5. The dotted lines represent the theoretical fracture resistance curves. $h/H = 1$, $\delta_1/h = 2\times10^{-4}$, $\delta_c/h = 2\times10^{-2}$, $\hat{\sigma}/\sigma_y = 3.75$, $\sigma_y/E^{\#2} = 0.01$, $a_2/E^{\#2} = -0.2$, $E^{\#2}/E^{\#1} = 0.01$.

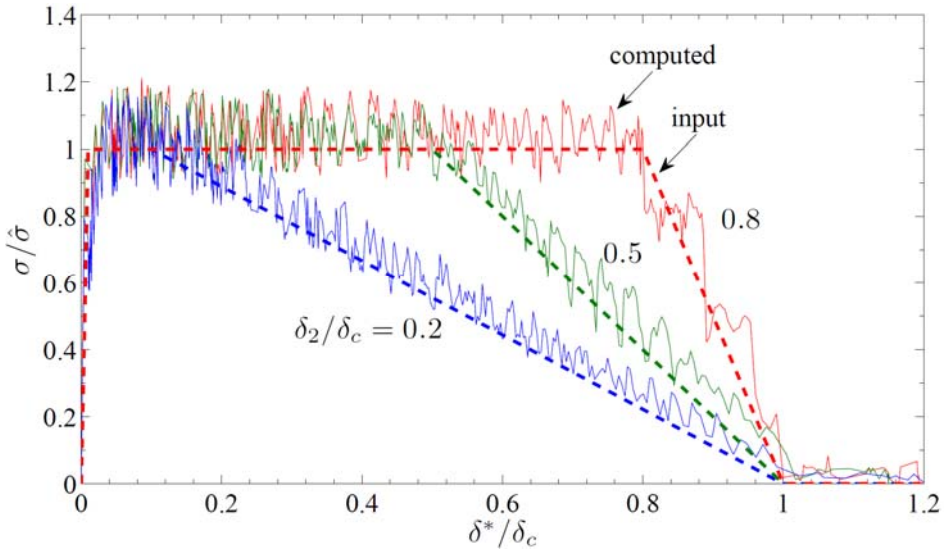


**Figure 6.** Calculated cohesive laws (solid lines) from $J_R$ and $\delta^*$ using Eq. 8. The model parameters are given in Fig. 5.

Fig. 7 shows the effect of the opening $\delta_2$ (see Fig. 1) on the steady-state fracture resistance for various ratios of peak cohesive traction over the initial yield stress of the non-linear material. For the range examined, the steady-state fracture resistance is only slightly larger than $J_c$. Secondly, the error in the stready-state fracture resistance decreases as the opening $\delta_2$ increases relatively to $\delta_c$. In all cases, the error in the steady-state fracture resistance

increases with increasing $\hat{\sigma}$; a larger ratio $\hat{\sigma}/\sigma_y$ means larger plastic dissipation around the cohesive zone.

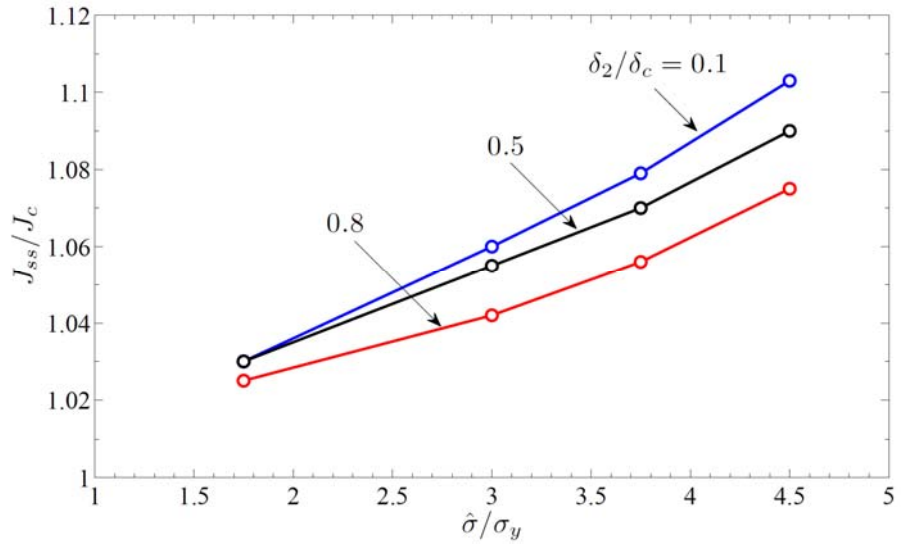


**Figure 7.** Normalized steady-state fracture resistance as a function of the cohesive peak stress normalized with the initial yield stress for three $\delta_2/\delta_c$ ratios. All other model parameters are given in Fig. 5.

Next in Fig. 8, the effect of the opening $\delta_c$ relative to the height $h$ is examined. A larger value of $\delta_c$ corresponds to a larger active cohesive zone size. As expected, when $\delta_c$ increases, the extent of the plastic zone increases and as a result the unloading region is larger. However, as in Fig. 7, the error in the calculated steady-state fracture resistance is below 11% for the range examined.

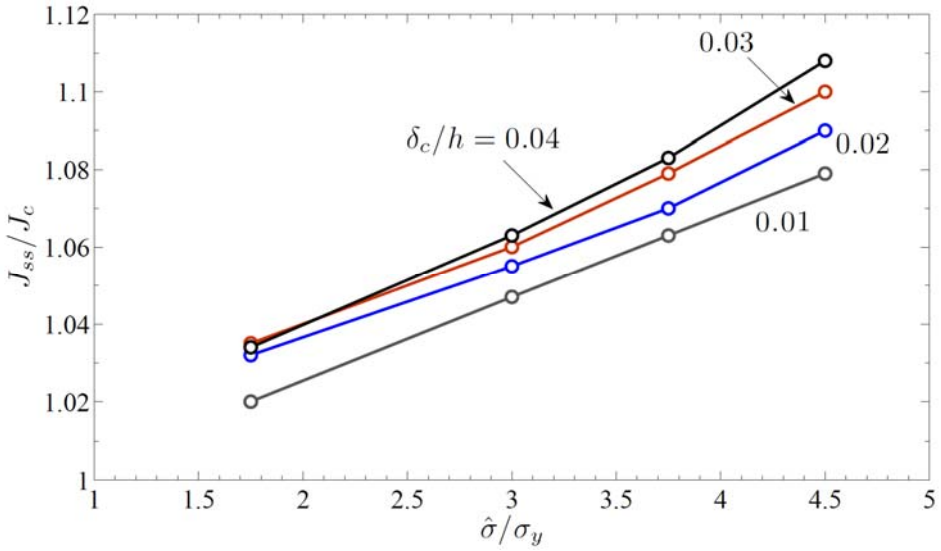


**Figure 8.** Normalized steady-state fracture resistance as a function of the cohesive peak stress normalized with the initial yield stress for three $\delta_c/h$ ratios. $\delta_2/h = 0.01$. All other model parameters are given in Fig. 5.

## 5. Conclusions

A test procedure to compute the fracture resistance and mode I cohesive law (peak traction, critical openings and shape) for materials with a non-linear stress-strain relationship was

developed. The method is based on a *J* integral specimen (Double Cantilever Beam sandwich specimen loaded with pure bending moments) subjected to monotonically increasing moments. The requirement of no unloading at any material point is not fulfilled exact in a small region at the crack tip wake. However, in the range of material and specimen parameters examined (large plastic zone but relatively small plastic strains), it was shown that the error introduced is below 11%. This is smaller than the scatter usually observed in fracture mechanics experiments. Thus, it can be argued that the method can be used in practice to determine fracture resistance and cohesive law determinations with satisfactory accuracy for materials undergoing large scale plasticity.

## References

[1] M. F. Kaninen and C. H. Popelar. *Advanced fracture mechanics*. Oxford University Press, New York, 1995.

[2] D. S. Dugdale. Yielding of steel sheets containing slits. *Journal of the Mechanics and Physics of Solids*, 8:100-104, 1960.

[3] G. I. Barenblatt. The mathematical theory of equilibrium cracks in brittle fracture. *Advances in Applied Mechanics*, 77:55-129, 1962.

[4] A. Needleman. A continuum model for void nucleation by inclusion debonding. *Journal of Applied Mechanics*, 54:525-531, 1987.

[5] V. Tvergaard and J. W. Hutchinson. The relation between crack growth resistance and fracture process parameters in elastic plastic solids. *Journal of the Mechanics and Physics of Solids*, 40:1377-1397, 1992.

[6] Q. D. Yang, M. D. Thouless and S. M. Ward. Numerical simulations of adhesively-bonded beams failing with extensive plastic deformation. *Journal of the Mechanics and Physics of Solids*, 47:1337-1353, 1999.

[7] I. Mohammed and K. M. Liechti. Cohesive zone modeling of crack nucleation at bimaterial corners. *Journal of the Mechanics and Physics of Solids*, 48:735-764, 2000.

[8] B. N. Cox and D. B. Marshall. The determination of crack bridging forces. *International Journal of Fracture*, 49:159-176, 1991.

[9] P. Brenet and F. Conchin and G. Fantozzo and P Reynaud and D. Rouby and C. Tallaron. Direct measurement of the crack bridging tractions: a new approach of the fracture behavior of ceramic-matrix composites. *Composites Science and Technology*, 56:817-823, 1996.

[10] J. R. Rice. A path independent integral and the approximate analysis of strain concentrations by notches and cracks. *Journal of Applied Mechanics*, 35:379-386, 1968.

[11] V. C. Li and R. J. Ward. A novel testing technique for post-peak tensile behaviour of cementitious materials. In Fracture toughness and fracture energy-testing methods for concrete and rocks, H. Mihashi, H. Takahashi and F. H. Wittmann, 183-195. A. A. Balkema Publishers, Rotterdam, 1989.

[12] Z. Suo and G. Bao and B. Fan. Delamination R-curve phenomena due to damage. *Journal of the Mechanics and Physics of Solids*, 40:1-16, 1992.

[13] B. F. Sørensen and T. K. Jacobsen. Large-scale bridging in composites: R-curves and bridging laws. *Composites Part A - Applied Science and Technology*, 29: 1443-1451, 1998.

[14] S. Goutianos, R. Arévalo, B. F. Sørensen and T. Peijs. Delamination R-curve phenomena due to damage. *Applied Composite Materials*, DOI 10.1007/s10443-013-9381-0, 2014.